ORGANIC CHEMISTRY FRONTIERS

CCS 中国化学会 CHINESE CHEMICAL SOCIETY

SIOC

ROYAL SOCIETY OF CHEMISTRY

π-Extended dibenzo[g,p]chrysenes

Journal:	*Organic Chemistry Frontiers*
Manuscript ID	QO-RES-01-2021-000068.R1
Article Type:	Research Article
Date Submitted by the Author:	17-Feb-2021
Complete List of Authors:	Hossain, Mohammad Mosharraf; Miami University, Chemistry and BioChemistry Mirzaei, M. Saeed; Razi University, Chemistry Lindeman, Sergey; Marquette University, Department of Chemistry Mirzaei, Saber; University of Pittsburgh, Chemistry Rathore, Rajendra; Marquette University, Department of Chemistry

ARTICLE

π-Extended dibenzo[*g*,*p*]chrysenes

Mohammad Mosharraf Hossain,*§[a] M. Saeed Mirzaei,[b] Sergey V. Lindeman,[a] Saber Mirzaei,*[c] and Rajendra Rathore‡[a]

Received 00th January 20xx,
Accepted 00th January 20xx

DOI: 10.1039/x0xx00000x

Here, we report two series (denoted *meta* and *para*) of π-extended dibenzo[*g*,*p*]chrysenes (DBC) with different substituents (H, Me and OMe). These six novel compounds benefit from the presence of eight methyl groups on the sp^3 bridges which improve solubility and rigidify the extended phenylenes. Optoelectronic properties were determined using electrochemistry and spectroscopic (UV-vis and emission) techniques and further supported by DFT calculations. The results showed that both the position and nature of substituents on the π-extended moieties exert significant effects on optoelectronic properties and the charge delocalization mechanism. In addition, isomerism (*meta* and *para*) leads to different packing in structure in the solid state; interestingly, the crystal structure of the hydrogen substituted *para* molecule showed a permanent three-dimensional porous structure.

Introduction

Polycyclic aromatic hydrocarbons (PAHs) with both flat and twisted/contorted structures have been of ever growing interest to chemists over the past century.[1-12] Among this superfamily, dibenzo[*g*,*p*]chrysene (DBC) constitutes a unique class of PAHs with a twisted topology (Chart 1).[13] Regarding this molecule, substantial investigations have been done both in terms of developing the synthetic strategies[14-19] and demonstrating interesting properties.[20-24] In an early attempt by our group, the isolation and the first insights into electronic structure of octasubstituted DBC were achieved.[25] Therein, the role of frontier molecular orbitals (FMO) in the bond length alteration of octamethoxy DBC (*meta* and *para* positions, Chart 1) upon the one-electron oxidation potential was highlighted. In a separate study, we introduced a highly efficient route toward the synthesis of skeletal DBC using DDQ as the oxidant.[16] Also, we investigated the dependence of the frontier molecular orbital energies/shapes on substituent positions.[26]

More recently, the Iwasawa group reported the site-selective synthesis of DBC derivatives including the controlled hydroxylation of *para* and *meta* (Chart 1) regions of DBC.[27] The same group synthesized twofold alkylated DBCs and observed that the two remaining sites accept groups selectively.[28] Regarding electronic structure, Liu et al. reported that electron-rich/deficient substitutions markedly change the photophysical properties of DBC.[29] Moreover, the substituted DBC fragment shows interesting features in the solid state and is useful in the preparation of liquid crystals.[30-32]

Despite these efforts, to our best knowledge, the effects of the position (*meta* and *para*) and/or substituents of π-extended DBC molecules on optoelectronic properties have not been explored. Herein, we employed two tetra-brominated DBC isomers and a practical two-step synthesis to obtain two different π-extended and rigid DBC species (Chart 1) with different substituents. Further, we investigate the optoelectronic properties of all compounds by employing both experimental (UV-vis, emission, electrochemistry) and computational methods.

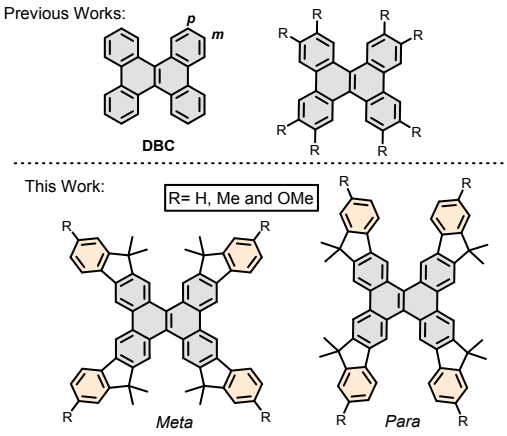

Chart 1. The structure of DBC and previously reported functionalized DBCs at different *meta* and/or *para* positions; π-extended DBC compounds in this work.

[a] *Department of Chemistry, Marquette University, Milwaukee, WI 53201-1414, United States. E-mail: hossaimm@miamioh.edu*
[b] *Department of Organic Chemistry, Faculty of Chemistry, Razi University, Kermanshah, Iran.*
[c] *Department of Chemistry, University of Pittsburgh, Pittsburgh, PA 15260, United States. E-mail: saber.mirzaei@pitt.edu*
§ Present Address: Miami University, Department of Chemistry & Biochemistry, Oxford, Ohio 45056, United States.
‡ Deceased February 16, 2018.

Electronic Supplementary Information (ESI) available: containing procedures for the synthesis of compounds; $^1H/^{13}C$ NMR spectra; crystal structures (CCDC numbers 2039941-2039944); computational details. See DOI: 10.1039/x0xx00000x

Results and discussion

Synthesis

The gram-scale synthesis of tetra-brominated *meta* and *para* DBCs can be done in good to excellent yields following a reported procedure (see ESI for details).[33] In order to install the aryl groups, we synthesized three different 3,3-dimethyl-benzoxaborole compounds with H, Me and OMe substituents (**A** in Scheme 1) following literature procedures.[34-36] These groups on compound **A** allow us to investigate substituent effects on optoelectronic properties. The installation of **A** on the tetra-Br DBCs was accomplished using the $Pd(dppf)Cl_2$ as a catalyst in a 2:1 mixture of 1,2-dimethoxyethane (DME) and water in 33-98% yields. This relatively large range can be attributed to the different solubilities of intermediate species (e.g., two or three additions). The tetrahydroxy species were obtained without column chromatography and characterized by ^1H NMR and HRMS techniques (see ESI for further details). These tetrahydroxy compounds were subjected to oxidative cyclization using methanesulfonic acid (CH_3SO_3H) in anhydrous CH_2Cl_2 for ~2 hours. The presence of Me groups on the sp^3 bridging carbons, in addition of making the reaction feasible by stabilizing the carbocation, allow us to rigidify the products and help to improve the solubility. The final products were purified using silica gel column chromatography or recrystallization and characterized using $^1H/^{13}C$ NMR and MALDI-TOF spectroscopies. We have also obtained single-crystal structures of four out of six final compounds (***p*-H**, ***m*-H**, ***m*-Me** and ***m*-OMe**) which unambiguously show the targeted products.

Crystallography

Slow evaporation of a 1,2-dichloroethane solution of ***p*-H** and 1:1 dichloromethane/acetonitrile solutions of ***m*-H, *m*-Me** and ***m*-OMe** at room temperature afforded high-quality crystals. As expected, all compounds possess twisted topologies inherited from the DBC backbone. Comparison of ***p*-H** with ***m*-H** (Fig. 1) shows similar bond distances with negligible differences (~10 pm). Also, there are no significant structural changes due to the different substituents of the *meta* isomer; the single-crystal structures of ***m*-Me** and ***m*-OMe** are provided in the supporting information (Fig. S1, ESI).

The packing patterns of ***p*-H** and ***m*-H** differ dramatically. The ***p*-H** molecules are interlocked with their neighbours through scissor-like arms via CH···π (~2.77–3.55 Å) interactions. The assembly extends along the c axis and constructs a microporous structure that is held together purely by noncovalent interactions (Fig. 1). The narrow opening of the channel has a rectangular shape with a size of 6.3×5.8 Å; considering the van der Waals radius of carbon (1.7 Å)[37] the dimensions decrease to 2.9×2.4 Å. Also, as depicted in Fig. 1, the dominant noncovalent interactions are CH···π (~2.53 Å) for ***m*-H**.

Recently, Meng et al. introduced π-stacked organic frameworks (termed π-OF) with improved features (e.g. solubility and conductivity) over conventional covalent organic frameworks (COF).[38] We believe that our compound (***p*-H**) can be classified in this new class of organic frameworks (π-OF) and has a very high potential to be further explored in this different field of materials chemistry.

The distance between the ring centroids (π-π distance) is larger than 4.7 Å for both the ***m*-H** and ***p*-H** isomers and the rings are not parallel with respect to each other. To the contrary, both ***m*-Me** and ***m*-OMe** showed π-π stacking with parallel-displaced configurations. The extended phenylenes interact with the DBC backbone with the center-to-center distance of ~3.8 Å for both ***m*-Me** and ***m*-OMe** (Fig. S2, ESI). Also, the distance of the least-squares-fit planes (angle between two planes is < 1°) of the parallel rings is ~3.5 Å (Fig. S3 and S4, ESI). This value is in perfect agreement with the computationally calculated distance (3.5 Å)[39] for benzene/benzene dimer in a parallel-displaced geometry and matches the accepted distance range (3.4-3.8 Å) for π-π interactions;[40] note that this geometry is around 1.15 kcal/mol more stable than the sandwich-stacked geometry for benzene/benzene dimer.[41]

Spectroscopy

The oxidation potentials of all π-extended DBCs were collected using a platinum electrode for ~1×10^{-3} M solutions containing 0.1 M tetra-butylammonium hexafluorophosphate (n-Bu_4NPF_6) as the supporting electrolyte. The cyclic voltammograms of all DBCs met the criteria of reversibility for the oxidation process (Fig. 2). The first oxidation potential of unsubstituted/unextended dibenzochrysene (DBC) is around 0.88 V vs Fc/Fc^+.[26] Comparing this value with the ***m*-H** (E_{ox1} = 0.53 V vs Fc/Fc^+) and ***p*-H** (E_{ox1} = 0.70 V vs Fc/Fc^+) reveals that the extended π systems in both *meta* and *para* isomers can decrease the first oxidation potential; however, this decrease depends highly on the position of the connected phenylene moiety.[26] Moreover, the *para*-substituted DBCs exhibit a significantly higher oxidation potential compared to *meta* isomers. Interestingly, with the increase of the electron-donating nature of the phenylene moieties (from H to Me to

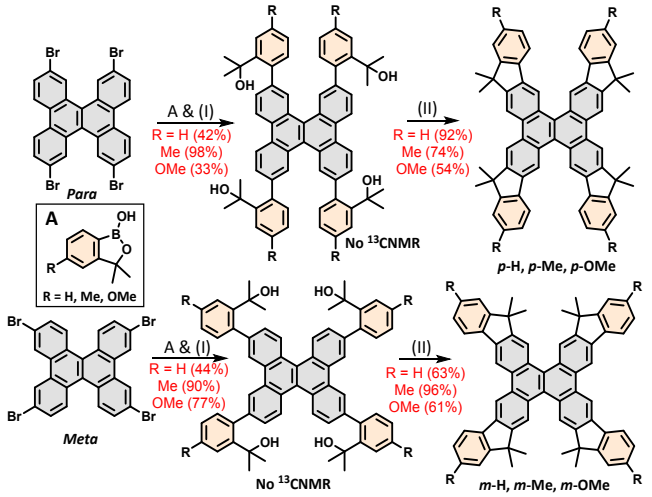

Scheme 1. Synthesis of *para* and *meta* compounds. Reaction conditions: (I) $Pd(dppf)Cl_2$, Na_2CO_3, 2:1 DME/H_2O, 100 °C; (II) CH_3SO_3H, CH_2Cl_2, rt.

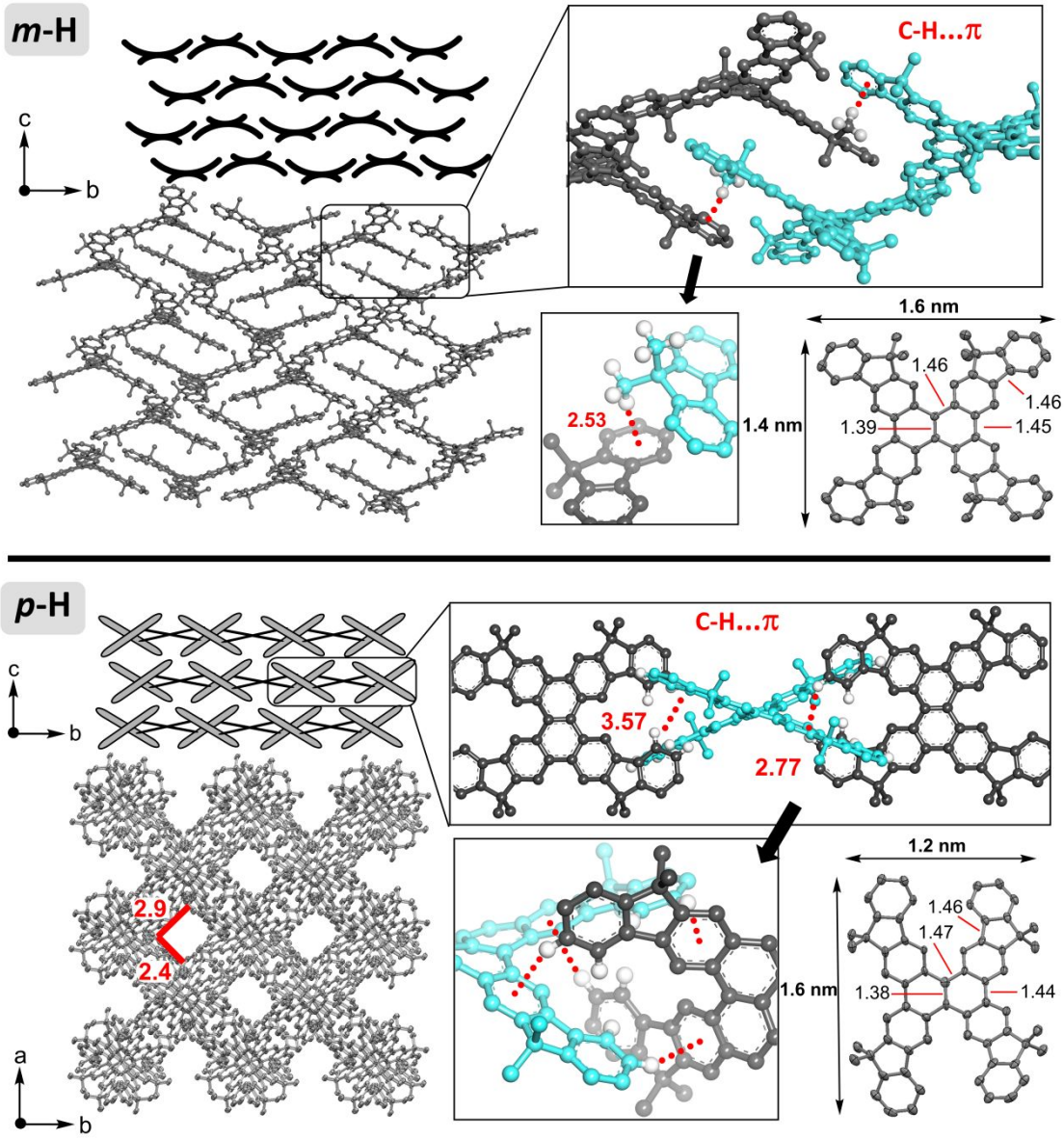

Fig. 1 The schematic, ball-stick representation of crystal packing arrangment and CH···π interactions (in angstrom, Å) of *m*-H (top) and *p*-H (down). Crystal structures obtained at 100 K; hydrogen atoms and solvent molecules are deleted for clarity and thermal ellipsoids are set at 50% probability level.

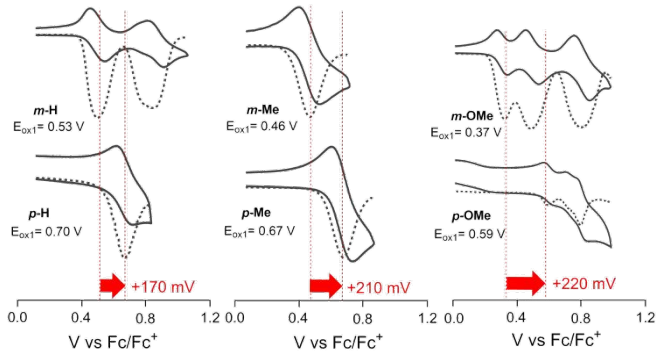

Fig. 2 Cyclic (—) and square-wave (···) voltammograms of *para* and *meta* substituted isomers of DBCs in a solution of CH_2Cl_2 (containing 0.1 M *n*-Bu_4NPF_6) at a scan rate of 200 mV/s and room temperature.

OMe), the difference between *meta* and *para* isomers increases significantly. This difference is around 170, 210 and 220 mV for H, Me and OMe, respectively. This is in accordance with the observation from our previous study that substitution of four methoxy groups on the *meta* or *para* positions of the DBC core decreases the first oxidation potentials to 0.40 and 0.73 V, respectively. The major difference is that π-extended ***p*-OMe** decreases the first oxidation potential by ~140 mV more efficient than tetramethoxy directly connected to the *para* positions of DBC core.[26] To the contrary, this value is just ~30 mV for *meta* species, indicating weaker effects of the extended π systems on the *meta* isomers relative to their *para* counterparts.

The absorption and emission spectra of both isomers were collected to provide a better understanding of their electronic

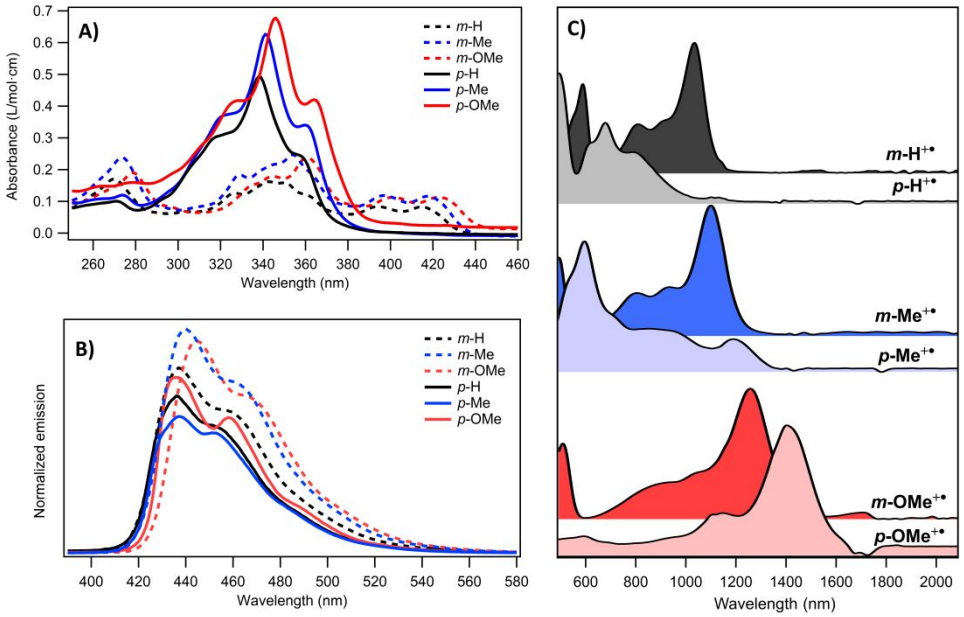

Fig. 3 UV-vis absorption (A) and emission (B) spectra of *meta* (···) and *para* (—) DBCs at neutral state in CH_2Cl_2 and room temperature. (C) UV-vis-Near IR absorption spectra of *meta* (dark colors) and *para* (light colors) DBCs$^{+\bullet}$ at 0 °C.

Table 1. Experimental and DFT (in parentheses) values of the first oxidation potential (E_{ox1}, V vs Fc/Fc^+), maximum absorption (maximum of the lowest transition peak, nm) and emission (nm), energy of HOMO (calculated using $E_{HOMO} = -[E_{1/2} + 4.80]$ eV) and LUMO (eV, calculated using $E_g = E_{LUMO} - E_{HOMO}$) and optical gap ($E_g$, eV, calculated using the offset wavelength, see the ESI for more details).

Compound	E_{ox1} (V vs Fc/Fc^+)	Absorption (nm)[a]	Absorption (CR, nm)	Emission (nm)	E_{HOMO} (eV)[b]	E_{LUMO} (eV)[b]	E_g (eV)[c]
m-H	0.53	415 (396)	1040 (893)	437	-5.33 (-5.98)	-2.49 (-1.55)	2.84 (4.43)
m-Me	0.46	417 (399)	1106 (958)	440	-5.26 (-5.88)	-2.43 (-1.48)	2.83 (4.40)
m-OMe	0.37	422 (402)	1233 (1075)	445	-5.17 (-5.77)	-2.38 (-1.41)	2.79 (4.37)
p-H	0.70	357 (327)	800 (618)	436	-5.50 (-6.25)	-2.20 (-1.25)	3.30 (5.00)
p-Me	0.67	360 (331)	1207 (1192)	438	-5.47 (-6.18)	-2.22 (-1.18)	3.25 (5.00)
p-OMe	0.59	364 (335)	1414 (1388)	435	-5.39 (-6.04)	-2.23 (-1.16)	3.16 (4.88)

In parentheses are: [a] DFT maximum absorption (λ_{max} nm); [b] DFT energy of HOMO (eV) and [c] DFT E_g (E_{LUMO}–E_{HOMO}, eV); all DFT values are reported at MN15/6-31+G(d,p)+PCM(CH_2Cl_2) level of theory.

structures. Fig. 3A and 3B display the absorption and emission spectra of the DBCs in their neutral state. As expected, by increasing the electron-donating ability of the substituent, the absorption spectrum red-shifted for both isomers; however, this shift is not significant (~2-7 nm). The position of the attached π system does make a significant difference between *meta* and *para* species (~58 nm regardless of the substituent). Having these data, we calculated optical gaps (E_g) for both series using the absorption edge wavelength ($\lambda_{a.e}$, see the computational details, ESI).[42] As listed in Table 1, the E_g of the *meta* isomers are around 0.4 eV smaller than those of the *para* isomers. Moreover, the electrochemistry data are used to calculate the E_{HOMO} according to $E_{HOMO} = -[E_{1/2} + 4.80]$ eV, where $E_{1/2}$ is the first redox event.[43] Finally, the E_{LUMO} of all species wascalculated by using $E_g = E_{LUMO} - E_{HOMO}$.

Unlike the absorption spectra, all six compounds have very similar emission spectra (λ_{em} = 435-445 nm). These similar λ_{em}s lead to a notable difference between Stokes shift values. While the *meta* compounds exhibit small Stokes shifts (~1200 cm^{-1}), the *para* species show much bigger values (~4800 cm^{-1} on average). The Stokes shifts are important when thinking about the practical applications of PAHs as optical materials; compounds with larger Stokes shifts benefit from lower self-quenching.[44, 45]

In order to complement our data about the different electronic structures of our compounds, we examined the absorption spectra of the cation radical species, generated by quantitative redox titrations using $THEO^{\bullet+}SbCl_6^-$ (E_{red} = 0.67 V vs Fc/Fc^+ and λ_{max} = 518 nm) for ***p*-OMe**, ***m*-H**, ***m*-OMe** and ***m*-Me** and $NAP^{\bullet+}SbCl_6^-$ (E_{red} = 0.94 V vs Fc/Fc^+ and λ_{max} = 672 nm) for ***p*-H** and ***p*-Me** as oxidants in CH_2Cl_2 at 0 °C (Fig. 3C).[46] The lower temperatures were used to decrease noise and measurements at room temperature showed no change of the spectra despite reduced noise. The absorption spectra of the *meta* isomers showed very similar patterns among different substituents (H, Me and OMe). However, as listed in Table 1, and opposite to the neutral species, these substituents have larger effects (~100 nm) on the absorption spectra. Comparing the *meta* DBCs with their *para* isomers, there are remarkable differences. While the λ_{max} is higher for ***m*-H** (1040 vs 800 nm), both ***m*-Me** (λ_{max} = 1106 nm) and ***m*-OMe** (λ_{max} = 1233 nm) showed lower values in comparison with their *para* isomer;

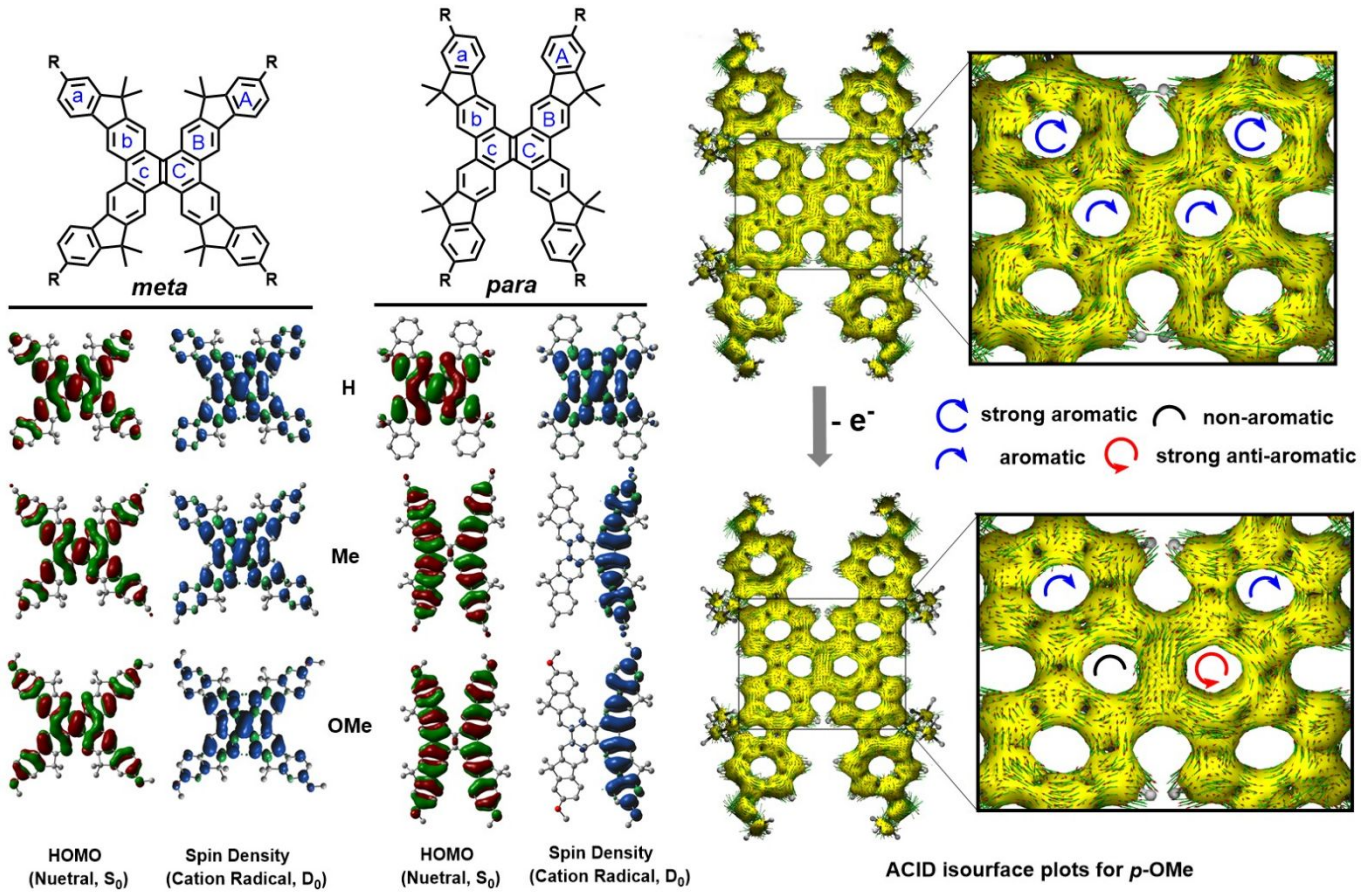

Fig. 4 Left: ring labels for NICS calculations and corresponding isosurface representations (±0.02 au) of HOMO (neutral, S_0) and spin density (±0.001 au, cation radical, D_0) for *meta* and *para* DBCs obtained at MN15/6-31+G(d,p)+PCM(CH_2Cl_2) level. Right: ACID isosurface plots (0.05) of *p*-OMe DBC in the neutral and oxidized states. The induced ring current vectors are plotted inside the rings to denote the diatropic and paratropic ring currents.

λ_{max} is 1207 and 1414 nm for ***p*-Me** and ***p*-OMe**, respectively. These data illustrate abnormal effects that not only suggest a different electronic structure among the *para* species, but also reveal a clear difference between the *meta* and *para* isomers. To understand these phenomena and gaining better insights about these novel species, we employed computational techniques.

Computational

The calculated energies at the MN15/6-31+G**+PCM(CH_2Cl_2) level of theory showed that the *meta* isomers are more stable than their *para* counterparts in the neutral (ΔG = 1 kcal mol^{-1}) and one-electron oxidized states (ΔG = 5-8 kcal mol^{-1}). We calculated these values using five different functionals (see the computational details, ESI); the results showed that these relative energies are independent of the employed functional (Table S2, ESI).

The calculated HOMO/LUMO energies show bigger gaps (E_g) for *para* versus *meta* isomers (Table 1) which agree with the experimental data; however, the DFT calculations overestimate (~1.5 eV) the E_g. This overestimation is not related to the selected functional and all other examined methods showed the same trend (Table S3, ESI). TD-DFT calculations can reproduce the experimental data with acceptable accuracy. Analysis of the TD-DFT data showed that for *meta* isomers the major contribution (~94%, oscillator strength ≈ 1.0) of the highest transition (396-402 nm) comes from the HOMO-to-LUMO transition. However, for *para* isomers, the HOMO-to-LUMO transition has either no (***p*-H** and ***p*-OMe**) or smaller contributions (~51%, ***m*-Me**) to the λ_{max} values (Table 1).

Evaluating the frontier molecular orbitals of our compounds reveals that while the HOMOs of the *meta* isomers have similar patterns for different substituents (i.e. HOMO is distributed over the whole aromatic system), the *para* isomers show two different patterns (Fig. 4). The HOMO is mainly distributed over the DBC backbone in the ***p*-H** molecule and does not have any contribution from the extended phenylene groups. By contrast, the ***p*-Me** and ***p*-OMe** HOMOs have totally different shapes and distributions. Also, note that the large HOMO contribution over the central C-C bond of DBC is decreased dramatically (from ~24% to ~1%) by moving from ***p*-H** to ***p*-Me**/***p*-OMe**. This effect can decrease electronic communication between the two sides by making a nodal

Table 2. NICS values for OMe substituted of *meta* and *para* DBC isomers calculated at MN15/6-31+G**+PCM(CH_2Cl_2) level; the values for H and Me substituents are provided in the Table S5, ESI.

Ring	a	b	c	A	B	C
***m*-OMe**						
Neutral	-7.8	-6.8	-1.4	-7.8	-6.8	-1.4
CR	-7.2	-2.3	5.3	-7.2	-2.3	5.3
***p*-OMe**						
Neutral	-7.9	-6.8	-1.4	-7.9	-6.8	-1.4
CR	-7.8	-5.3	0.1	-5.6	-5.4	11.0

planeand indeed separates two *p*-quaterphenyl moieties electronically.

To further investigate the effects of these different patterns on hole stabilization, we calculated the spin densities of the cation radical spices (Fig. 4). For the *meta* compounds, the spin density is delocalized over the whole molecule and follows the HOMO pattern. The same result is observed for the ***p*-H** molecule (i.e. spin density follows the HOMO pattern and the extended phenylenes have no contribution to charge stabilization). To the contrary, for the ***p*-Me** and ***p*-OMe** isomers the hole is localized on one side, which is similar to our previous study of *para*-tetramethoxy DBC.[26]

To classify our compounds according to the Robin-Day classification[47] of charged species, we calculated electronic couplings (V_{12}) and structural reorganization energies (λ_{reorg}, Fig. S5, ESI). Based on these data and looking at the spin density distributions (Fig. S5 and Fig. 4), the *meta* isomers are class III (strong electronic coupling, evenly and static charge delocalization, $2V_{12} > \lambda_{reorg}$), while the para compounds have smaller electronic coupling than the reorganization energy and are clas II ($\lambda_{reorg} > 2V_{12}$).

This different charge (de)localization behaviour explains the different UV-vis-NIR spectra. As listed in Table 1, the TD-DFT calculations reproduce the experimental data with good accuracy; however, similar to the neutral compounds, the TD-DFT results showed systematic underestimation. These calculations revealed that the highest transition (~1600 and 2200 nm for *meta* and *para* isomers, respectively) which is from HOMO-to-LUMO, has a very weak oscillator strength and the observed λ_{max} is originating from transitions involving other orbitals (Fig. S6-S17, ESI).

Further, the analysis of the C–C bond lengths of oxidized *para* isomers confirms that single bonds between *p*-quaterphenyl moieties undergo contraction only on one side with the Me and OMe substituents (Fig. S18, ESI). However, the bond alteration and the shape of the orbitals provide no strong evidence of aromatic to quinoidal switching from the neutral to cation radical states.

Finally, in order to investigate the aromaticity changes of our systems upon oxidation, aromaticity descriptors were utilized.[48-50] Nucleus-independent chemical shift (NICS)[51, 52] calculations indicate the extent of local aromaticity, with negative values for aromatic systems and positive values for antiaromatic rings. As listed in Table 2, for neutral compounds the aromaticity pattern is symmetric and relatively identical for both *meta* and *para* isomers. At the oxidized state, the extended phenylenes (A/a rings, Fig. 4) remain aromatic with small changes, but the DBC rings undergo dramatic changes. For example, when oxidizing to the cation radical (CR) the NICS values of the B/b and C/c rings of the ***m*-OMe** molecule indicate large shifts from -6.8 to -2.3 and from -1.4 to +5.3, respectively. These aromaticity changes are symmetrical for the *meta* compounds (Table S5, ESI), but for the *para* isomers with Me and OMe substituents, the loss of aromatic character in the DBC core is more dramatic and asymmetric. For example, for ***p*-OMe,** the shift is -6.8 to -5.4 in ring B, -1.4 to +11.0 in ring C and -1.4 to +0.1 in ring c. These values show more antiaromatic character in the side where the hole has been localized.

In addition to NICS calculations, the analysis of the anisotropy of the current induced density (ACID)[53] method confirms the significant aromaticity disturbance upon oxidation (Fig. 4). The substantial clockwise ring current in the A/a and B/b sites of the neutral state and current vectors in the opposite direction for the C/c ring indicates the strong aromatic and non-aromatic character, respectively, which follow the Clar sextet rules.[54] On one-electron oxidation, ring C becomes antiaromatic, with a counter-clockwise ring current, while the adjacent c ring keeps its very weak aromatic nature. Therefore, the NICS and ACID data reveal that in the π-extended DBCs both substituent structures and their positions can tune the aromaticity of oxidized species.

Conclusions

Here we developed two different series (denoted *meta* and *para*) of π-extended dibenzo[*g*,*p*]chrysenes (DBC) with different substituents (H, Me and OMe). The final compounds are rigid and showed good solubility owing to the presence of bridged sp^3 carbons. The developed synthetic method is not restricted to the investigated substituents and can easily be extended to different groups. These six molecules are designed to investigate the effects of both extended aromaticity and substituents on the optoelectronic properties of DBCs. Interestingly, the experimental (electrochemistry and UV-vis) and DFT data showed strong effects of both substituent position (*meta* vs *para*) and structure on the charge delocalization mechanism. In addition, the *p*-H compound showed interesting packing in the solid state which generate a permanent porosity purely through C-H···π interactions. Applications of this porous compound will be published in due course. The results of this study can be useful in the different fields of materials chemistry and can shed light on the importance of substituent effects on π-conjugated systems and charge delocalization in PAHs.

Conflicts of interest

There are no conflicts to declare.

Acknowledgements

The authors would like to thank Prof. Scott A. Reid (Marquette University), Prof. C. Scott Hartley (Miami University) and Prof.

Raúl Hernández Sánchez (University of Pittsburgh) for helpful discussions and encouragement. We also thank the NSF (CHE-1508677) for financial support. We thank Dr. Bhaskar Godugu at University of Pittsburgh for the HRMS data. S.M. thanks the Dietrich School of Arts & Sciences Graduate Fellowship.

Notes and references

1 M. M. Haley and R. R. Tykwinski, *Carbon-Rich Compounds: From Molecules to Materials*, WILEY-VCH Verlag GmbH & Co, Weinheim, 2006.
2 G. Povie, Y. Segawa, T. Nishihara, Y. Miyauchi and K. Itami, Synthesis of a carbon nanobelt, *Science*, 2017, **356**, 172-175.
3 C. Liu, M. E. Sandoval-Salinas, Y. Hong, T. Y. Gopalakrishna, H. Phan, N. Aratani, T. S. Herng, J. Ding, H. Yamada, D. Kim, D. Casanova and J. Wu, Macrocyclic Polyradicaloids with Unusual Super-ring Structure and Global Aromaticity, *Chem*, 2018, **4**, 1586–1595.
4 J. He, J. L. Crase, S. H. Wadumethrige, K. Thakur, L. Dai, S. Zou, R. Rathore and C. S. Hartley, ortho-Phenylenes: Unusual Conjugated Oligomers with a Surprisingly Long Effective Conjugation Length, *J. Am. Chem. Soc.*, 2010, **132**, 13848–13857.
5 S. Mirzaei, E. Castro and R. H. Sánchez, Tubularenes, *Chem. Sci.*, 2020, **11**, 8089–8094.
6 A. Boddeda, M. M. Hossain, M. S. Mirzaei, S. V. Lindeman, S. Mirzaei and R. Rathore, Angular ladder-type meta-phenylenes: synthesis and electronic structural analysis, *Org. Chem. Front.*, 2020, **7**, 3215–3222.
7 T. S. Navale, M. V. Ivanov, M. M. Hossain and R. Rathore, FHBC, a Hexa-peri-hexabenzocoronene–Fluorene Hybrid: A Platform for Highly Soluble, Easily Functionalizable HBCs with an Expanded Graphitic Core, *Angew. Chem. Int. Ed.*, 2018, **57**, 790–794.
8 A. Narita, X.-Y. Wang, X. Feng and K. Müllen, New advances in nanographene chemistry, *Chem. Soc. Rev.*, 2015, **44**, 6616–6643
9 M. Ball, Y. Zhong, Y. Wu, C. Schenck, F. Ng, M. Steigerwald, S. Xiao and C. Nuckolls, Contorted Polycyclic Aromatics, *Acc. Chem. Res.*, 2015, **48**, 267–276.
10 K. Y. Cheung, Y. Segawa and K. Itami, Synthetic Strategies of Carbon Nanobelts and Related Belt-Shaped Polycyclic Aromatic Hydrocarbons, *Chem. Eur. J.*, 2020, **26**, 14791–14801.
11 Y. Segawa, H. Ito and K. Itami, Structurally uniform and atomically precise carbon nanostructures, *Nat. Rev. Mater.*, 2016, **1**, 15002.
12 M. Hermann, D. Wassy and B. Esser, Conjugated Nanohoops Incorporating Donor-, Acceptor-, Hetero- or Polycyclic Aromatics, *Angew. Chem. Int. Ed.*, 2020, DOI: 10.1002/anie.202007024.
13 R. E. Buckles, A. Serianz and D. Naffziger, Dibenzo(*g,p*) Chrysene: A Challenging Experiment in Organic Synthesis, *Proc. Iowa Acad. Sci.*, 1973, **80**, 45–49.
14 N. Suzuki, T. Fujita and J. Ichikawa, Method for the Synthesis of Dibenzo[*g,p*]Chrysenes: Domino Friedel–Crafts-Type Cyclization of Difluoroethenes Bearing Two Biaryl Groups, *Org. Lett.*, 2015, **17**, 4984–4987.
15 S. Yamaguchi and T. M. Swager, Oxidative Cyclization of Bis(biaryl)acetylenes: Synthesis and Photophysics of Dibenzo[*g,p*]chrysene-Based Fluorescent Polymers, *J. Am. Chem. Soc.*, 2001, **123**, 12087–12088.
16 T. S. Navale, K. Thakur and R. Rathore, Sequential Oxidative Transformation of Tetraarylethylenes to 9,10-Diarylphenanthrenes and Dibenzo[*g,p*]chrysenes using DDQ as an Oxidant, *Org. Lett.*, 2011, **13**, 1634–1637.
17 M. Shimizu, I. Nagao, Y. Tomioka and T. Hiyama, Palladium-Catalyzed Annulation of vic-Bis(pinacolatoboryl)alkenes and -phenanthrenes with 2,2′-Dibromobiaryls: Facile Synthesis of Functionalized Phenanthrenes and Dibenzo[*g,p*]chrysene*s*, *Angew. Chem. Int. Ed.*, 2008, **47**, 8096–8099.
18 Y. Shoji, N. Tanaka, S. Muranaka, N. Shigeno, H. Sugiyama, K. Takenouchi, F. Hajjaj and T. Fukushima, Boron-mediated sequential alkyne insertion and C–C coupling reactions affording extended π-conjugated molecules, *Nat. Commun.*, 2016, **7**, 12704.
19 X. Zhang, Z. Xu, W. Si, K. Oniwa, M. Bao, Y. Yamamoto and T. Jin, Synthesis of extended polycyclic aromatichydrocarbons by oxidative tandem spirocyclizationand 1,2-aryl migration, *Nat. Commun.*, 2017, **8**, 15073.
20 Y. Suzuki, N. Tohnai, A. Saeki and I. Hisaki, Hydrogen-bonded organic frameworks of twisted polycyclic aromatic hydrocarbon, *Chem. Commun.*, 2020, **56**, 13369–13372.
21 N. Keller, T. Sick, N. N. Bach, A. Koszalkowski, J. M. Rotter, D. D. Medina and T. Bein, Dibenzochrysene enables tightly controlled docking and stabilizes photoexcited states in dual-pore covalent organic frameworks, *Nanoscale*, 2019, **11**, 23338–23345.
22 Y. Ueda, H. Tsuji, H. Tanaka and E. Nakamura, Synthesis, Crystal Packing, and Ambipolar Carrier Transport Property of Twisted Dibenzo[g,p]chrysenes, *Chem. Asian J.*, 2014, **9**, 1623–1628.
23 M. Ren, J. Wang, X. Xie, J. Zhang and P. Wang, Double-Helicene-Based Hole-Transporter for Perovskite Solar Cells with 22% Efficiency and Operation Durability, *ACS Energy Lett.*, 2019, **4**, 2683–2688.
24 X.-S. Ke, Y. Hong, V. M. Lynch, D. Kim and J. L. Sessler, Metal-Stabilized Quinoidal Dibenzo[*g,p*]chrysene-Fused Bis-dicarbacorrole System, *J. Am. Chem. Soc.*, 2018, **140**, 7579–7586.
25 T. S. Navale, L. Zhai, S. V. Lindeman and R. Rathore, Octamethoxydibenzochrysene: isolation and X-ray crystallographiccharacterization of a twisted polyaromatic cation radical, *Chem. Commun.*, 2009, 2857–2859.
26 M. V. Ivanov, M. R. Talipov, T. S. Navale and R. Rathore, Ask Not How Many, But Where They Are: Substituents Control Energetic Ordering of Frontier Orbitals/Electronic Structures in Isomeric Methoxy-Substituted Dibenzochrysenes, *J. Phys. Chem. C.*, 2018, **122**, 2539–2545.
27 N. Yoshida, S. Kamiguchi, K. Sakao, R. Akasaka, Y. Fujii, T. Maruyama and T. Iwasawa, Regio-defined multi-hydroxylation of Dibenzo[*g,p*]chrysene, *Tetrahedron Lett.*, 2020, **61**, 152033–152036.
28 N. Yoshida, S. Kamiguchi, Y. Fujii, K. Sakao, T. Maruyama, S. Tokai, Y. Matsumoto, Y. Taguchi, R. Akasaka and T. Iwasawa, Straightforward synthetic routes to well-soluble and regio-defined dibenzo[*g,p*]chrysene derivatives, *Tetrahedron Lett.*, 2020, **61**, 152406–152410.
29 C.-W. Li, C.-I. Wang, H.-Y. Liao, R. Chaudhuri and R.-S. Liu, Synthesis of Dibenzo[*g,p*]chrysenes from Bis(biaryl)acetylenes via Sequential ICl-Induced Cyclization and Mizoroki−Heck Coupling, *J. Org. Chem.*, 2007, **72**, 9203−9207.
30 S. Kumar and S. K. Varshney, Dibenzo[*g,p*]chrysene, a Novel Core for Discotic Liquid Crystals, *Mol. Cryst. Liq. Cryst.*, 2002, **378**, 59–64.
31 R. Chaudhuri, M.-Y. Hsu, C.-W. Li, C.-I. Wang, C.-J. Chen, C. K. Lai, L.-Y. Chen, S.-H. Liu, C.-C. Wu and R.-S. Liu, Functionalized Dibenzo[*g,p*]chrysenes: Variable Photophysical and Electronic Properties and Liquid−Crystal Chemistry, *Org. Lett.*, 2008, **10**, 3053–3056.

32 S. K. Varshney, H. Nagayama, H. Takezoe and V. Prasad, Octasubstituted Dibenzochrysenes: Discotic Liquid Crystals with a Twisted Core, *Liq. Cryst.*, 2009, **36**, 1409−1415.

33 X.-Y. Liu, X. Tang, Y. Zhao, D. Zhao, J. Fan and L.-S. Liao, Dibenzo[*g,p*]chrysene: A New Platform for Highly Efficient Red Phosphorescent Organic Light-Emitting Diodes, *Dyes Pigm.*, 2017, **146**, 234−239.

34 S. Kusano, S. Miyamoto, A. Matsuoka, Y. Yamada, R. Ishikawa and O. Hayashida, Benzoxaborole Catalyst for Site-Selective Modification of Polyols, *Eur. J. Org. Chem.*, 2020, 1598–1602.

35 T. Akama, Y. R. Freund, P. W. Berry, D. S. Carter, E. E. Easom, K. Jarnagin, C. S. Lunde, J. J. Plattner, F. Rock, R. Stefanakis, C. Fischer, C. A. Bulman, K. C. Lim, B. M. Suzuki, N. Tricoche, A. Mansour, U. DiCosty, S. McCall, B. Carson, J. W. McCall, J. McKerrow, M. P. Hübner, S. Specht, A. Hoerauf, S. Lustigman, J. A. Sakanari and R. T. Jacobs, Macrofilaricidal Benzimidazole–Benzoxaborole Hybrids as an Approach to the Treatment of River Blindness: Part 1. Amide Linked Analogs, *ACS Infect. Dis.*, 2020, **6**, 173–179.

36 W. H. Parsons, R. R. Calvo, W. Cheung, Y.-K. Lee, S. Patel, J. Liu, M. A. Youngman, S. L. Dax, D. Stone, N. Qin, T. Hutchinson, M. L. Lubin, S.-P. Zhang, M. Finley, Y. Liu, M. R. Brandt, C. M. Flores and M. R. Player, Benzo[d]imidazole Transient Receptor Potential Vanilloid 1 Antagonists for the Treatment of Pain: Discovery of trans-2-(2-{2-[2-(4-Trifluoromethyl-phenyl)-vinyl]-1H-benzimidazol-5-yl}-phenyl)-propan-2-ol (Mavatrep*)*, *J. Med. Chem.*, 2015, **58**, 3859–3874.

37 A. Bondi, van der Waals Volumes and Radii, *J. Phys. Chem.*, 1964, **68**, 441–451.

38 D. Meng, J. L. Yang, C. Xiao, R. Wang, X. Xing, O. Kocak, G. Aydin, I. Yavuz, S. Nuryyeva, L. Zhang, G. Liu, Z. Li, S. Yuan, Z.-K. Wang, W. Wei, Z. Wang, K. N. Houk and Y. Yang, Noncovalent π-stacked robust topological organic framework, *Proc. Natl. Acad. Sci.*, 2020, **117**, 20397–20403.

39 S. A. Arnsteina and C. D. Sherrill, Substituent effects in parallel-displaced π–π interactions, *Phys. Chem. Chem. Phys.*, 2008, **10**, 2646–2655.

40 C. Janiak, A critical account on π–π stacking in metal complexes with aromatic nitrogen-containing ligands, *J. Chem. Soc., Dalton Trans.*, 2000, 3885–3896.

41 J. M. Sanders, Optimal π-Stacking Interaction Energies in Parallel-Displaced Aryl/Aryl Dimers are Predicted by the Dimer Heavy Atom Coun*t*, *J. Phys. Chem. A.*, 2010, **114**, 9205–9211.

42 J. C. S. Costa, R. J. S. Taveira, C. F. R. A. C. Lima, A. Mendes and L. M. N. B. F. Santos, Optical Band Gaps of Organic Semiconductor Materials, *Opt. Matt.*, 2016, **58**, 51–60.

43 C. M. Cardona, W. Li, A. E. Kaifer, D. Stockdale and G. C. Bazan, Electrochemical Considerations for Determining Absolute Frontier Orbital Energy Levels of Conjugated Polymers for Solar Cell Applications, *Adv. Mater.*, 2011, **23**, 2367–2371.

44 P. D. Sala, N. Buccheri, A. Sanzone, M. Sassi, P. Neri, C. Talotta, A. Rocco, V. Pinchetti, L. Beverina, S. Brovelli and C. Gaeta, First demonstration of the use of very large Stokes shift cycloparaphenylenes as promising organic luminophores for transparent luminescent solar concentrators, *Chem. Commun.*, 2019, **55**, 3160–3163.

45 W. Ma, W. Li, M. Cao, R. Liu, X. Zhao and X. Gong, *LargeStokes-shift AIE fluorescent materials for high-performance luminescent solar concentrators*, *Org. Electron.*, 2019, **73**, 226–230.

46 M. R. Talipov and R. Rathore, in *Organic Redox Systems: Synthesis, Properties, and Applications*, ed. T. Nishinaga, John Wiley & Sons, Inc., Hoboken, New Jersey, 2015.

47 M. B. Robin and P. Day, Mixed Valence Chemistry-A Survey and Classification, *Adv. Inorg. Chem. Radiochem.*, 1968, **10**, 247–422.

48 T. M. Krygowski, H. Szatylowicz, O. A. Stasyuk, J. Dominikowska and M. Palusiak, Aromaticity from the Viewpoint of Molecular Geometry: Application to Planar Systems, *Chem. Rev.*, 2014, **114**, 6383–6422.

49 R. Gershoni-Poranne and A. Stanger, Magnetic criteria of aromaticity, *Chem. Soc. Rev.*, 2015, **44**, 6597-6615

50 Z. Zeng, X. Shi, C. Chi, J. T. L. Navarrete, J. Casado and J. Wu, Pro-aromatic and anti-aromatic π-conjugated molecules: an irresistible wish to be diradicals, *Chem. Soc. Rev.*, 2015, **44**, 6578–6596.

51 Z. Chen, C. S. Wannere, C. Corminboeuf, R. Puchta and P. v. R. Schleyer, Nucleus-Independent Chemical Shifts (NICS) as an Aromaticity Criterion, *Chem. Rev.*, 2005, **105**, 3842–3888.

52 P. v. R. Schleyer, C. Maerker, A. Dransfeld, H. Jiao and N. J. R. v. E. Hommes, Nucleus-Independent Chemical Shifts: A Simple and Efficient Aromaticity Probe, *J. Am. Chem. Soc.*, 1996, **118**, 6317–6318.

53 D. Geuenich, K. Hess, F. Köhler and R. Herges, Anisotropy of the induced current density (ACID), a general method to quantify and visualize electronic delocalization, *Chem. Rev.*, 2005, **105**, 3758–3772.

54 E. Clar, *The Aromatic Sextet*, Wiley, New York, 1972.